

Amplifier-in-the-Loop Adaptive Radar Waveform Synthesis

DYLAN EUSTICE

Numerica, Fort Collins, CO, USA

CASEY LATHAM

CHARLES BAYLIS, Senior Member, IEEE

ROBERT J. MARKS II, Fellow, IEEE

Baylor University, Waco, TX, USA

LAWRENCE COHEN, Senior Member, IEEE

Radar Division, Naval Research Laboratory, Washington, DC, USA

Adaptive algorithms having the capacity to perform real-time optimization in response to a dynamic environment will be necessary for the development of a cognitive radar technology. This paper details an amplifier-in-the-loop algorithm to synthesize radar waveforms which are optimized for desired ambiguity function characteristics in a monostatic radar system, with constraints on the peak-to-average power ratio and spectrum of the waveform. The algorithm uses alternating projections to search for a waveform whose ambiguity function best approximates the goal for a volume-based constraint in desired regions of the range–Doppler plane. Results are shown for both simulation and measurement cases, both with and without the effects of a nonlinear amplifier. This waveform synthesis method is expected to be useful in real-time adaptive radar systems.

Manuscript received March 22, 2016; revised July 5, 2016 and September 12, 2016; released for publication September 13, 2016. Date of publication February 7, 2017; date of current version April 27, 2017.

DOI. No. 10.1109/TAES.2017.2665158

Refereeing of this contribution was handled by S. D. Blunt

This work was supported by a grant from the National Science Foundation under Award ECCS-1343316.

Authors' addresses: D. Eustice is with Numerica, Fort Collins, CO 80528 USA, E-mail: (Dylan_Eustice@baylor.edu); C. Latham, C. Baylis, and R. J. Marks II are with the Department of Electrical and Computer Engineering, Baylor University, Waco, TX 76798-7356 USA, E-mail: (Casey_Latham@baylor.edu; Charles_Baylis@baylor.edu; Robert_Marks@baylor.edu); L. Cohen is with the Radar Division, Naval Research Laboratory, Washington DC 20375-5320 USA, E-mail: (lawrence.cohen@nrl.navy.mil).

0018-9251 © 2017 IEEE

I. INTRODUCTION

As the number of wireless devices grows and the amount of spectrum available for radar applications diminishes, there will be a growing need for adaptive and reconfigurable radar systems. In order to realize this goal, algorithms are needed which can provide real-time optimization to quickly maximize efficiency and spectral compliance in situations where the relative range and Doppler of radar targets are changing, while maintaining the high quality of performance expected of military or civilian radar systems. The overall performance of a radar system includes different parameters which are often intrinsically linked, leading to many tradeoffs which must be considered when applying optimization. Fundamentally, the main criteria when evaluating a radar system are: spectral compliance, power efficiency, and range/Doppler resolution capability. The range/Doppler resolution capability is assessed using the well-known ambiguity function (AF) associated with the transmitted waveform. An adaptive waveform synthesis algorithm is presented that considers all three of these criteria, as well as the distortion effects of a nonlinear power amplifier. The algorithm uses an alternating projections approach to provide real-time optimization of a waveform's AF under constraints of the synthesized waveform's peak-to-average power ratio (PAPR) and a required spectral mask, while also attempting to negate the effects of the nonlinear amplifier on the emission's spectra and AF using basic predistortion techniques.

First derived by Woodward [1], the AF is a 2-D function describing the detection capabilities of a waveform. The AF is the output of the matched filter that performs the correlation operation in the radar at differences in range and Doppler from the actual range and Doppler of the target [2], [3]. It is mathematically defined as

$$\chi(\tau, u) = \int_{-\infty}^{\infty} x(t) x^*(t - \tau) e^{-j2\pi ut} dt \quad (1a)$$

where $x(t)$ is the associated temporal waveform, τ is the relative delay, and u is the relative Doppler frequency. Equivalently

$$\chi(\tau, u) = \int_{-\infty}^{\infty} X(f + u) X^*(f) e^{j2\pi ft} df \quad (1b)$$

where $X(u)$ and $x(t)$ are Fourier transform pairs

$$X(u) = \mathcal{F}\{x(t)\} = \int_{-\infty}^{\infty} x(t) e^{-j2\pi ut} dt.$$

Note that this is sometimes depicted as the *auto-AF* to distinguish it from its counterpart used in bistatic radar systems, the cross-ambiguity function (CAF). More detailed information about the AF and its derivation from first principles can be found in a comprehensive overview by Eustice *et al.* [3].

Radar waveform synthesis with an optimized AF has been a topic of study since early 1960s. Noteworthy early work includes a classic synthesis technique derived by Wilcox [4], who uses a least squares estimation approach

to construct a waveform made up of a set of basis functions whose CAF approximates some goal CAF. Sussman [5] extends this work by devising methods which prevent the algorithm from being limited to the approximation of only functions with Hermitian symmetry and unity energy, as Wilcox does. Wolf *et al.* [6] provide another alternative for CAF synthesis using basis functions and pattern search, but only considers the class of phase-modulated waveforms. More recently, Gladkova and Chebanov [7], [8] have provided an extension to Wilcox’s method with the goal of improving its practicality; however, their solution involves using Hermite waveforms, whose generation may not be very straightforward, in practice [9], [10]. Sebt *et al.* [9] provide an extension to Sussman’s method which produces orthogonal frequency-division multiplexed with lowered PAPR for AF approximation. Additionally, Costas [11] presents a class of waveforms which attempt to mimic the ideal “thumbtack” shape of AFs, where there is a sharp main lobe and the AF magnitude in the remainder of the range–Doppler region is very small. Patton and Rigling have shown joint optimization of the waveform and receive filter to satisfy autocorrelation and cross-correlation constraints [12], synthesis of a waveform based on a desired Fourier spectrum [13], and waveform optimization to meet autocorrelation and modulus constraints [14].

Using projections in waveform synthesis algorithms is a technique which has been shown to be successfully utilized in previous literature. Selesnick and Pillai [15], [16] have used an alternating projections method to synthesize notched chirps for intermodulation cancelling. Kassab *et al.* [17] also use alternating projections to synthesize radar waveforms, but do so with a focus on the waveforms autocorrelation properties without considering the entire plane of the AF. Blunt *et al.* [18]–[21] present a useful method which also employs projections and an amplifier-in-the-loop approach to design radar waveforms. These works focus on using a continuous-phase-modulation scheme to optimize the integrated (ISL) and peak (PSL) sidelobe level of the waveforms along the zero-Doppler cut of the synthesized waveform’s AF. It is noted that these metrics can be expanded to other cuts in the range–Doppler plane, but even so, the detection benefits will mostly be seen in the nearby range resolution for this implementation. In a more recent work, Jakobosky *et al.* [22] use projections to design waveforms with tapered amplitude and a desired power density. These waveforms are emitted using a linear amplification using nonlinear components architecture, which is required to efficiently and properly transmit the waveforms synthesized. Nobakht and Civanlar [23] use projections to ensure lower a signal has lower signal strength in certain regions of its time and frequency domain. Bin *et al.* [24] also use projections in an algorithm which generates a constant modulus waveform, given a desired Fourier transform magnitude for the waveform. Similar to these approaches is the Gerchberg–Saxton algorithm, which allows the complete waveform to be synthesized, given the time- and frequency-domain magnitude information [25]. The Gerchberg–Saxton approach has been applied for

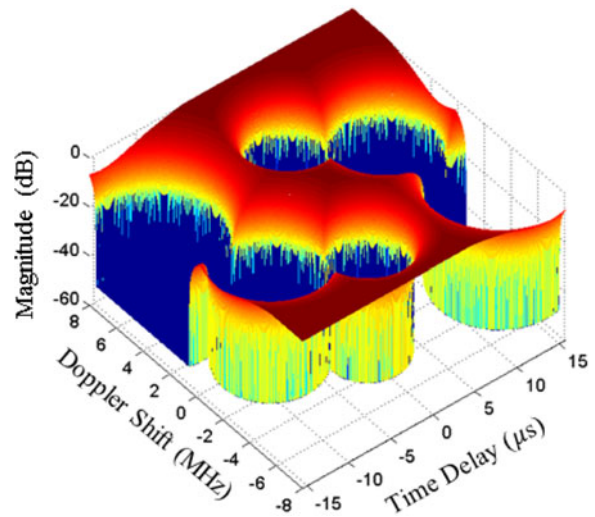


Fig. 1. Example of a minimization function. Existing in the range–Doppler domain, the minimization function acts as a limit for the magnitude of the desired AF at every (τ, u) within the support of the AF. In this example, the optimum AF will be minimized in the circular regions which have been depressed to about -50 dB.

synthesis of radar waveforms with desirable autocorrelation and cross-correlation properties [26].

Many of these works evaluate the quality of a waveform’s AF using metrics that evaluate the range or Doppler resolution, such as ISL or PSL, attempt to minimize the difference between the synthesized AF and a goal function, or seek to provide a general AF used for any environment. Our previous work [27], [28] introduces the minimization function, which provides a more general form on which to optimize the synthesized waveform’s AF. The minimization function is a 2-D function in the range–Doppler domain which serves as the optimization goal for the synthesis algorithm. Fig. 1 shows an example of a minimization function. Here, the minimization function has three depressions which are reflected in the way an AF is axially symmetric [3]. These depressions indicate where we wish to minimize the AF. The regions desired for minimization of the AF may be located at, for example, range–Doppler combinations of potentially interfering targets or clutter that would impede the ability to read the desired target, which is located at $(0, 0)$ on the AF’s range–Doppler plane. The derivation of the minimization function from system level considerations, however, is beyond the scope of this paper and is left for future analysis and demonstration.

We wish for the normalized AF magnitude to be constrained by the minimization function. In other words, we seek to find a waveform $x(t)$ with an associated AF $\chi(\tau, u)$ such that

$$\frac{|\chi(\tau, u)|}{|\chi(0, 0)|} \leq M(\tau, u), \quad \begin{matrix} -B \leq u \leq B \\ -T \leq \tau \leq T \end{matrix} \quad (2)$$

where B is the given frequency support of the waveform and T is the temporal support of the waveform.

A previous paper from our group [27] introduces the projections algorithm which lays out the fundamental

projections used to optimize the AF. Later work [28] expands on this optimization by allowing for requirements on the synthesized waveform's PAPR and spectral magnitude. This paper further expands the algorithm's practicality in a radar system by incorporating the nonlinearities of the transmitter power amplifier device into the waveform synthesis and by showing the algorithm's robustness in a dynamic environment by demonstrating adaptability to real-time changes in the minimization function and bandwidth requirements. While it shows some similarities to existing methods of waveform optimization above, the method we present is different from these methods. It differs, for example, from the pioneering work of Patton and Rigling [12]–[14] in that the entire ambiguity domain is considered. In addition, our work has been verified by simulation and in the laboratory.

Section II outlines the projection process used in the algorithm, the distance functions which evaluate AF quality, and the basic predistortion technique used. Section III describes simulation results of the algorithm, and Section IV provides results from measurement testing of the algorithm. Finally, Section V provides conclusions based on the presented results.

II. ALGORITHM DETAILS

In (2), the criteria for an optimum AF given a goal minimization function M were defined. Because the foundational basis of the algorithm is rooted in projections, the optimization problem will be defined using set theory. Let \mathcal{Z} be the set of all temporal waveforms having energy E , time support T , and frequency support B . Note that the time and frequency supports need not contain the entire time duration nor frequency bandwidth of the signal, respectively. A signal cannot be both time and frequency limited. However, the time support T and frequency support B should contain the entire time and frequency ranges, respectively, for which the AF is to be computed. Let \mathcal{X} be the set of all AFs, noting that, to within a constant phase term, there is a one-to-one mapping relationship between \mathcal{Z} and \mathcal{X} . The minimization function $M(\tau, u)$ will define the set \mathcal{M} , which is made up of 2-D functions in the range–Doppler domain which have a magnitude less than $M(\tau, u)$ for every combination of τ and u . Additionally, we define a set \mathcal{P} containing a class of waveforms with a PAPR less than the desired PAPR Γ and a set \mathcal{S} of all waveforms with a spectral magnitude which does not exceed a given spectral mask $S_m(f)$. Note that $\mathcal{P}, \mathcal{S} \subset \mathcal{Z}$. Therefore, we wish to find some waveform

$$x(t) \in \mathcal{P} \cap \mathcal{S} : x(t) \mapsto \mathcal{X} \cap \mathcal{M}. \quad (3)$$

There are a total of five different projections used, each of which will now be covered, before outlining the algorithm as a whole. The first projection $P_{\mathcal{M}}(\cdot)$ projects from the set of AFs \mathcal{X} to the set of minimized functions \mathcal{M} . It is done simply by enforcing the minimization criteria on the current AF, $\chi_i(\tau, u)$, by scaling the magnitude of the regions where (2) is not satisfied. The projection is

expressed as

$$\begin{aligned} \Phi_i(\tau, u) &= P_{\mathcal{M}}(\chi_i) \\ &= \begin{cases} \chi_i(\tau, u) \frac{M(\tau, u)}{|\chi_i(\tau, u)|}, & (\tau, u) \in B \\ \chi_i(\tau, u), & (\tau, u) \notin B \end{cases} \end{aligned} \quad (4)$$

where B is the set of (τ, u) where (2) is not satisfied. The result of the projection is $\Phi_i(\tau, u)$, a possibly complex, 2-D function in the range–Doppler space.

Next, an estimate for the waveform whose AF most closely resembles $\Phi_i(\tau, u)$ must be made. To do this, a projection to the 1-D time-domain set \mathcal{Z} is made. This projection is developed using concepts from [3] and [29], where we see that the AF may be inverted to within a scaling constant, which will briefly be shown. Starting from the AF definition in (1a), we note that $\chi(\tau, u)$ is the Fourier transform of $x(t)x^*(t - \tau)$. Taking the inverse Fourier of both sides and setting $t = 0$, we are left with

$$\int_{-\infty}^{\infty} \chi(\tau, u) du = x(0)x^*(-\tau).$$

After some trivial manipulation, the equation reduces to

$$x(\tau) = \frac{1}{x^*(0)} \int_{-\infty}^{\infty} \chi^*(-\tau, u) du. \quad (5)$$

A similar procedure uses the frequency-domain definition of the AF in (1b) to show that

$$X(u) = \frac{1}{X^*(0)} \int_{-\infty}^{\infty} \chi(t, u) dt. \quad (6)$$

If the 2-D function χ in (5) and (6) is in \mathcal{X} , the two inversions will result in two 1-D waveforms which are a Fourier transform pair. However, in the projections process, these inversions will be applied to $\Phi_i(\tau, u)$, for which $\Phi_i \notin \mathcal{M} \cap \mathcal{X} \rightarrow \Phi_i \notin \mathcal{X}$. In other words, if the optimization criterion from (3) is not met, Φ_i will not be an AF, and the inversions shown in (5) and (6) cannot be expected to agree. Note that (5) projects along the u -axis, while (6) projects along the τ -axis; thus, the changes from $\chi_i \rightarrow \Phi_i$ will be more accurately represented by finding some combination of these two projections. This is done by applying a weighted combination of the two projections. The time and frequency projections of the minimized AF Φ_i are given as follows:

$$z_i^t(t) = P_{\mathcal{Z}}^t(\Phi) = \frac{1}{x_{i-1}^*(0)} \int_{-B}^B \Phi_i^*(-\tau, u) du \quad (7a)$$

$$z_i^f(f) = P_{\mathcal{Z}}^f(\Phi) = \mathcal{F}^{-1} \left\{ \frac{1}{X_{i-1}^*(0)} \int_{-T}^T \Phi_i(\tau, u) d\tau \right\} \quad (7b)$$

where \mathcal{F}^{-1} denotes the inverse Fourier transform

$$x(t) = \mathcal{F}^{-1}\{X(u)\} = \int_{-\infty}^{\infty} X(u) e^{j2\pi ut} du.$$

The weights for each waveform are then calculated by taking the mean-square error between χ_i and Φ_i in the

direction of each corresponding projection

$$W^t = \int_{-T}^T \left| \int_{-B}^B \chi_i(\tau, u) - \Phi_i(\tau, u) du \right|^2 d\tau \quad (8a)$$

$$W^f = \int_{-B}^B \left| \int_{-T}^T \chi_i(\tau, u) - \Phi_i(\tau, u) d\tau \right|^2 du. \quad (8b)$$

The time-domain weighted combination of these projections is given by

$$\hat{x}_i(t) = P_Z(\Phi_i) = W^t z_i^t(t) + W^f z_i^f(t) \quad (9)$$

after which $\hat{x}_i(t)$ is normalized to energy E .

The final step to generate a candidate waveform is to ensure $x(t) \in \mathcal{P} \cap \mathcal{S}$. This is done via a separate alternating projections process $A_{\mathcal{P}, \mathcal{S}}(\hat{x})$. If the energy and PAPR are given, as they are here, the PAPR calculation may be inverted to find the maximum value associated with that waveform

$$C = \sqrt{\frac{1}{T} E \cdot 10^{\frac{1}{10} \Gamma}} \quad (10)$$

where C is the maximum value and Γ is assumed to be given in decibel. Define the set of all waveforms with maximum value C as \mathcal{C} and waveforms with energy E as \mathcal{E} . Thus, $\mathcal{E} \cap \mathcal{C} \subset \mathcal{P}$ and the two-step projection to $\mathcal{E} \cap \mathcal{C}$ is given by

$$x_i^c(t) = P_{\mathcal{C}}(\hat{x}_i) = \begin{cases} \hat{x}_i(t) \frac{C}{|\hat{x}_i(t)|}, & |\hat{x}_i(t)| > C \\ \hat{x}_i(t), & |\hat{x}_i(t)| \leq C \end{cases} \quad (11a)$$

$$x_i^{\mathcal{E}}(t) = P_{\mathcal{E}}(\hat{x}_i) = x_i^c(t) \cdot \frac{E}{\int_0^T |x_i^c(t)|^2 dt} \quad (11b)$$

$$x_i^{\mathcal{P}}(t) = P_{\mathcal{P}}(\hat{x}_i) = P_{\mathcal{E}}(P_{\mathcal{C}}(\hat{x}_i)). \quad (11c)$$

The projection to \mathcal{S} is done in the frequency domain by simply enforcing the spectral mask, with optional padding, where it is exceeded by the spectral density of the waveform

Define

$$X_i^{\mathcal{S}}(f) = \begin{cases} \frac{S_m(f)}{\beta}; & |\hat{X}_i(f)| > S_m(f) \\ \hat{X}_i(f); & |\hat{X}_i(f)| \leq S_m(f) \end{cases} \quad (12)$$

so that

$$x_i^{\mathcal{S}}(t) = P_{\mathcal{S}}(\hat{x}_i) = \mathcal{F}^{-1}(X_i^{\mathcal{S}}(f))$$

where β is the optional padding and $\hat{X}_i(u)$ and $\hat{x}_i(t)$ are Fourier transform pairs. The projections process ensuring $x_i(t) \in \mathcal{P} \cap \mathcal{S}$ can, therefore, be written concisely as

$$x_i(t) = P_{\mathcal{S}}(P_{\mathcal{P}}(\hat{x})) \quad (13)$$

which iterates until $x_i(t) \in \mathcal{P} \cap \mathcal{S}$.

The predistortion operation will now be discussed. A very simple model based on a hyperbolic tangent will be used, a method which has been shown in the previous literature covering memory-less amplifier models [30], [31]. The point of the predistorter in this context is not to improve on significant advances that have been recently made in amplifier predistortion techniques, but to show that even a simple predistortion technique can have great benefits for negating the effects of nonlinear amplifiers on the AF of the

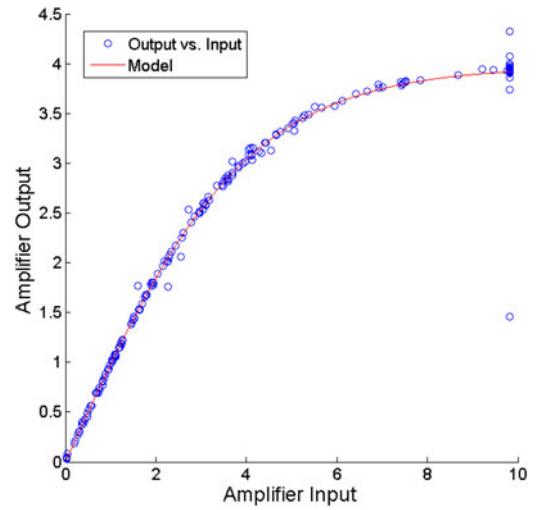


Fig. 2. Scatter plot used to determine the model for a given device and input waveform.

emission. The algorithm is not dependent on this selection of the prediction technique and any one of the wealth of advanced modern techniques [32]–[34] should be able to be used seamlessly. The model for the nonlinearities and its inverse are expressed as

$$y(t) = a_1 \tanh(a_2 x(t)) \quad (14a)$$

$$x(t) = \frac{1}{a_2} \tanh^{-1} \left(\frac{1}{a_1} y(t) \right) \quad (14b)$$

where $x(t)$ is the system input and $y(t)$ is the system output. Because the characteristics of the device may be changing in a dynamic system, the coefficients defining the model a_1 and a_2 are recalculated each iteration. They are calculated such that the mean-square error between the model and the amplifier output is minimized

$$\min_{a_1, a_2} \|y(t) - a_1 \tanh(a_2 x(t))\|^2. \quad (15)$$

Fig. 2 shows an example of the model being fit to the input and output scatter plot from an amplifier. Note that the inversion follows directly from the amplifier model.

There are two types of penalty functions used to evaluate the quality of the AF: minimax mean-squared errors. The minimax is a measure of the worst-case error in the AF with respect to the minimization function, and the mean-square is a measure of the overall error. Both functions are a measure of the distance from \mathcal{X} to \mathcal{M} and use χ and Φ for the calculation. The minimax function is calculated with

$$D_m(\chi, \Phi) = \max_{(\tau, u) \in \mathcal{B}} \left| \frac{\chi(\tau, u)}{\chi(0, 0)} \right| - \left| \frac{\Phi(\tau, u)}{\Phi(0, 0)} \right| \quad (16)$$

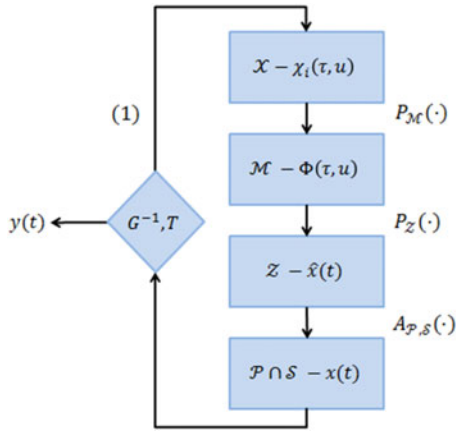


Fig. 3. Overview of the projections process. $P_M(\cdot)$ and $P_Z(\cdot)$ represent projections to \mathcal{M} and \mathcal{Z} , respectively, while $A_{P,S}(\cdot)$ is the multistep process of projections to find an $x(t) \in \mathcal{P} \cap \mathcal{S}$. (1) maps the temporal waveform $x(t)$ to its associated range–Doppler AF, while the waveform is selected with a decision process T and sent to the amplifier after passing through the predistortion model $G^{-1}(\cdot)$.

TABLE I
Summary of Sets Used in Alternating Projections Process

Set Name	Set Description
\mathcal{X}	Set of AFs
\mathcal{M}	Set of functions whose AF fits the minimization function template
\mathcal{Z}	Set of time-domain functions
\mathcal{P}	Set of functions meeting PAPR requirements
\mathcal{S}	Set of functions meeting spectral mask requirements

where \mathcal{B} is the set of (τ, u) where (2) is not satisfied. The mean-squares distance function is calculated via

$$D_s(\chi, \Phi) = \frac{1}{(4BT)^2} \int_{-T}^T \int_{-B}^B \left(\left| \frac{\chi(\tau, u)}{\chi(0, 0)} \right| - \left| \frac{\Phi(\tau, u)}{\Phi(0, 0)} \right| \right)^2 du d\tau. \quad (17)$$

The choice of the distance function to be used is left to the designer and what criterion is more important: overall matching or the worst-case detection scenario

$$D_m(\chi, \Phi) = \max_{(\tau, u) \in \mathcal{B}} \left| \frac{\chi(\tau, u)}{\chi(0, 0)} \right| - \left| \frac{\Phi(\tau, u)}{\Phi(0, 0)} \right|$$

$$D_s(\chi, \Phi) = \frac{1}{(4BT)^2} \int_{-T}^T \int_{-B}^B \left(\left| \frac{\chi(\tau, u)}{\chi(0, 0)} \right| - \left| \frac{\Phi(\tau, u)}{\Phi(0, 0)} \right| \right)^2 du d\tau.$$

Fig. 3 shows a block diagram of the projections process for the algorithm, and Table I summarizes the definitions of the sets described in the Fig. 3 projections process. The algorithm is initialized with $\chi_i(\tau, u) \in \mathcal{X}$, from which the projection is done to \mathcal{M} such that $\Phi_i(\tau, u) = P_M(\chi_i)$. The two-step projection process to the time-domain set \mathcal{Z} is done to generate waveform $\hat{x}_i(t) = P_Z(\Phi_i)$ where $\hat{x}_i(t)$ is an estimate of the candidate waveform $x_i(t)$ that may or

may not satisfy the required PAPR and spectral constraints. A multistep projections process $x_i(t) = A_{P,S}(\hat{x}_i)$ is then done to nudge the candidate waveform toward satisfying these constraints. After the candidate waveform is found, a decision-making process T is used to determine whether or not the candidate waveform will be selected as an emission. The selection process simply looks at the previous candidates generated since the most recent minimization function was created and selects the waveform that possesses the lowest associated distance function value for the current $M(\tau, u)$. The choice of using the minimax or least squares distance function in T is left to the user. The least squares function is used in the experimental results.

If the problem is overdefined such that the spectral constraints and the minimization function template cannot be well-accomplished, for example, the algorithm will provide the best AF (with respect to the minimization template) that meets the spectral mask and PAPR requirements. The spectrum and PAPR requirements projection is last, as shown in Fig. 3, so the result at the end of each iteration is required to meet these requirements, and may not adhere to the minimization template at the end of the loop. This is practically what is desired: obtaining the best AF possible for the scenario described by the minimization function while adhering to spectral requirements.

III. SIMULATION RESULTS

The algorithm is tested in simulations written in MATLAB. Three different experiments will be shown, with each experiment repeated twice: the first without accounting for simulated nonlinearities (no predistortion) and the second in which the nonlinearities are taken into account. The simulations use a hyperbolic tangent model defined by coefficients (a_1, a_2) to simulate the effects of memory-less nonlinearities from a high-power amplifier. The coefficients are unknown to the projections process and the nonlinear transfer function is applied to a quadrature-amplitude modulation (QAM) waveform, which is digitally modulated to the carrier frequency $F_c = 3.3$ GHz. The minimization functions are chosen to simulate a real-world environment in which a target being tracked has three potential interfering objects in its range–Doppler plane. A circular region of varying size and centered at the approximate location of the interfering object is depressed into the minimization function for each, as can be seen in Fig. 5. Note that, in general, these objects can move in the range–Doppler plane as a function of time, or in this case iteration number, due to differences in relative velocity and acceleration.

Each experiment continuously generates a 150-sample waveform over a period of 250 iterations. The time support $T = 9.375 \mu\text{s}$ and the frequency support $B = 8$ MHz. The required spectral mask for each experiment is shown (with 0 MHz being the center frequency of the waveform) in Fig. 4 and the required PAPR for each experiment is 2 dB. The minimization function is adjusted every ten iterations.

Additionally, a control waveform is constructed for comparison to illustrate the relative benefit of using the

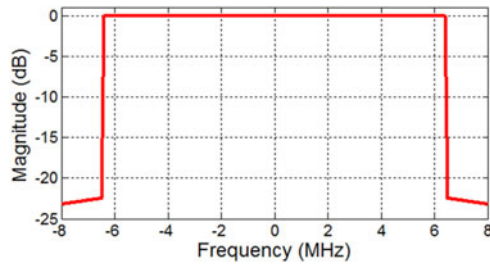


Fig. 4. Spectral mask required for waveform compliance in all experiments.

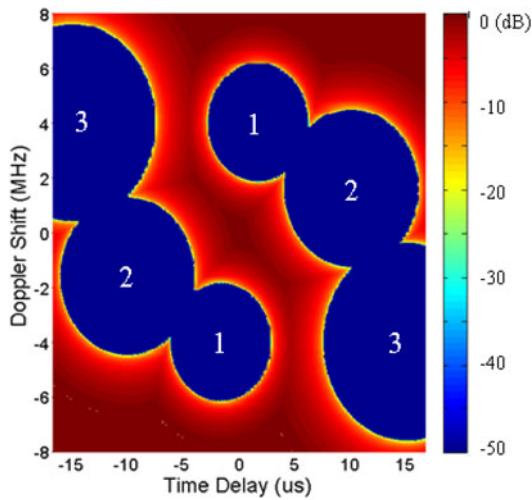


Fig. 5. Example of the depressions in the minimization function corresponding to potential interferers, which are labeled “1,” “2,” and “3.” Note the axial symmetry property of AF is enforced on the range–Doppler location of the objects.

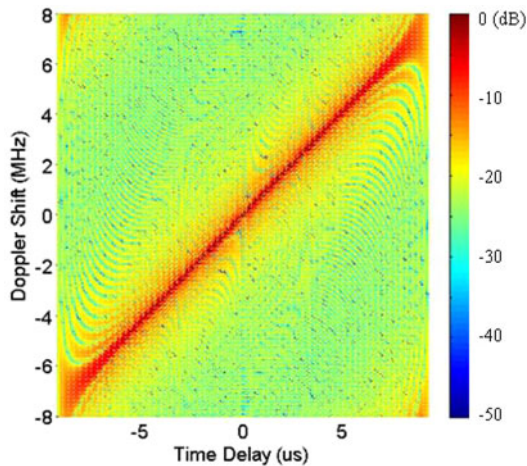


Fig. 6. AF of the LFM chirp used as a control function against which to test the waveforms produced in the experiments.

waveform produced by the projections algorithm. It is very common in radar applications to use a linear-frequency-modulated (LFM) chirp. An LFM chirp centered at 3.5 MHz and with a bandwidth of 7 MHz is used as the control waveform for comparison. The AF magnitude of the chirp function used as the control is shown in Fig. 6.

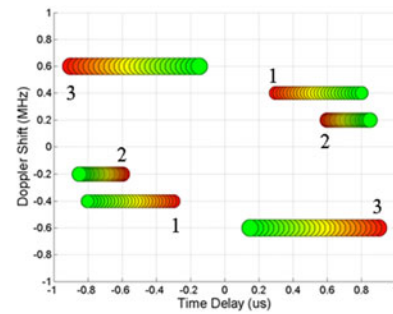


Fig. 7. Map for Experiment 1 showing the movement of potentially interfering objects through the range–Doppler plane relative to a target being tracked at the origin. The red circles indicate the starting location of the objects and the green circles indicate the ending location.

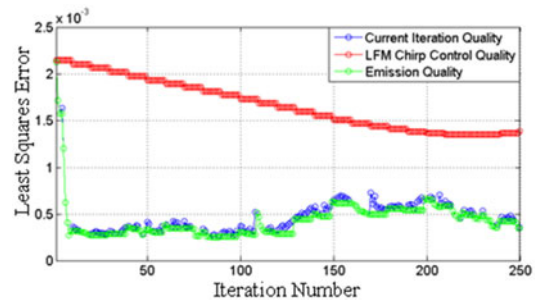


Fig. 8. Experiment 1 (Simulation), least squares distance quality as the algorithm iterates. The red circles show the distance quality for the control waveform, the green circles show the simulated emission, and the blue circles show the current iteration, as if T were not applied.

TABLE II
Simulation Results for Experiment 1

	Minimax		Least Squares $\cdot 10^{-3}$	
	Mean	Std. Dev.	Mean	Std. Dev.
Emission (Predistortion)	0.166	0.0618	0.433	0.214
Emission (No Predistortion)	0.175	0.0674	0.471	0.218
Control	0.689	0.0768	1.64	0.265

Experiment 1 assumes there are no acceleration differences between the target and the interfering objects. Fig. 7 shows a map of the objects’ movement through the range–Doppler plane in Experiment 1 as the algorithm iterates. Fig. 8 shows the values of the least squares distance function associated with the three relevant waveforms: the control waveform, the emission waveform, and the waveform at the current iteration. The results shown in Fig. 8 were generated with the simulated amplifier in the loop and waveform predistortion applied before simulating the emission. These are compared to both the control waveform and the emission when the model is not in the loop and predistortion is not applied in Table II. As the data in Table II and in Fig. 8 show the waveforms with and without predistortion have a much better distance function using both the minimax and the least squares distance function. In all cases, the minimax and least squares optimization results are more than a factor of 3 improvement. Practically, this means that the probability of a “false reading” from a target with range

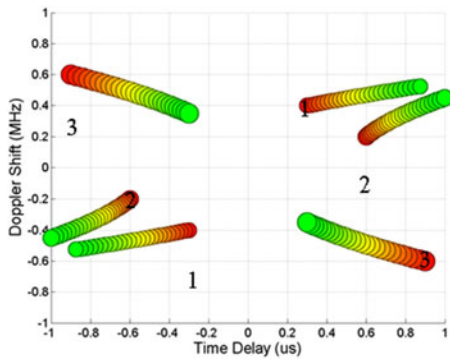


Fig. 9. Map for Experiment 2 showing the movement of potentially interfering objects through the range–Doppler plane relative to a target being tracked at the origin. The red circles indicate the starting location of the objects and the green circles indicate the ending location.

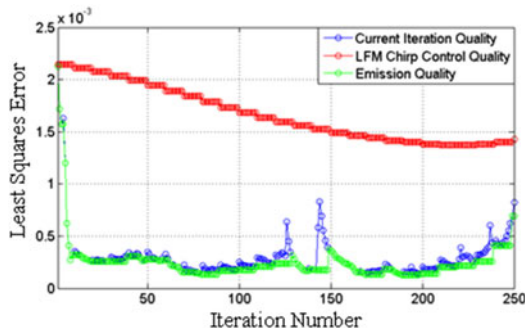


Fig. 10. Least squares distance quality versus iteration number for Experiment 2 (simulation) as the algorithm iterates. The red circles show the distance quality for the control waveform, green circles show the simulated emission, and the blue circles show the waveform at the current iteration, as if T were not applied.

and Doppler in the minimization regions being incorrectly read as possessing the range and Doppler at the origin is decreased by this factor. It can be seen in Fig. 8 that the least squares distance quality of the control LFM chirp waveform changes with iteration number even though this waveform is held constant; this is because the minimization function is changing as the algorithm iterates.

Experiment 2 has nonzero relative acceleration for all three interferers. One of the interferers has a negative relative acceleration, while the other two objects have positive relative accelerations. Fig. 9 shows a map of the objects' movement through the range–Doppler plane as the algorithm iterates, where the effects of the accelerations can be seen by the objects' vertical movement in the range–Doppler plane. Fig. 10 shows the least squares distance function for the predistorted waveforms and the control waveforms as the algorithm iterates, while Table III contains a summary of the results for Experiment 2. As with Experiment 1, it is clear that the waveforms produced by the projections algorithm have a much better distance functions than the control LFM chirp waveform. Additionally, as could be expected, the predistorted waveforms perform slightly better than the waveforms with no predistortion.

Experiment 3 also has nonzero relative accelerations for all three interferers, as well as different starting

TABLE III
Simulation Results for Experiment 2

	Minimax		Least Squares $\cdot 10^{-3}$	
	Mean	Std. Dev.	Mean	Std. Dev.
Emission (Predistortion)	0.196	0.109	0.253	0.220
Emission (No Predistortion)	0.207	0.106	0.280	0.237
Control	0.699	0.0692	1.66	0.260

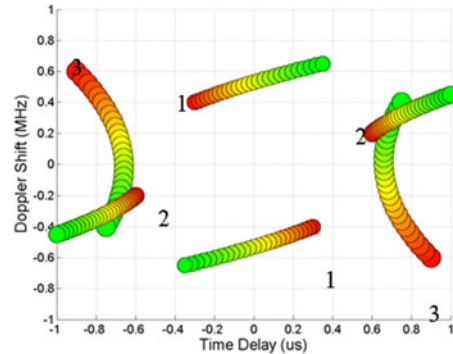


Fig. 11. Map for Experiment 3 showing the movement of potentially interfering objects through the range–Doppler plane relative to a target being tracked at the origin. The red circles indicate the starting location of the objects and the green circles indicate the ending location.

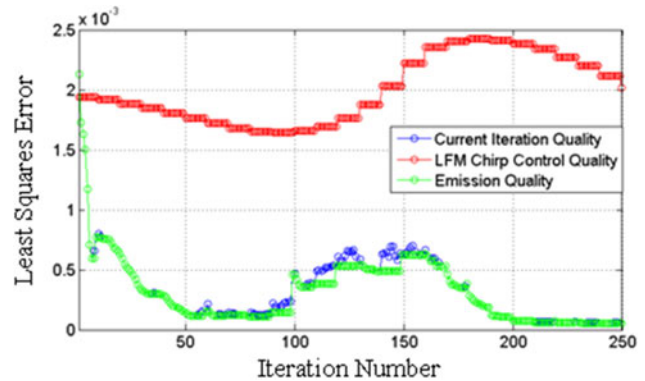


Fig. 12. Least squares distance quality versus iteration number for Experiment 3 (Simulation) as the algorithm iterates. The red circles show the distance quality for the control waveform, green circles show the simulated emission, and the blue circles show the waveform at the current iteration, as if T were not applied.

locations. Again, one interferer has a negative relative acceleration, while the other two have positive relative accelerations. Fig. 11 shows a map of the objects' movement through the range–Doppler plane as the algorithm iterates, Fig. 12 shows the least squares distance function for the relevant waveforms, and Table IV provides a summary of the results.

IV. MEASUREMENT RESULTS

The algorithm was also tested using a nonlinear test bench in the laboratory of the authors. Fig. 13 shows a block diagram of the measurement setup. As with the simulations, the computations for the algorithm are all performed in MATLAB, which supplies the digital waveforms to the

TABLE IV
Simulation Results for Experiment 3

	Minimax		Least Squares $\cdot 10^{-3}$	
	Mean	Std. Dev.	Mean	Std. Dev.
Emission (Predistortion)	0.138	0.0758	0.320	0.287
Emission (No Predistortion)	0.163	0.0864	0.390	0.312
Control	0.697	0.0445	2.00	0.278

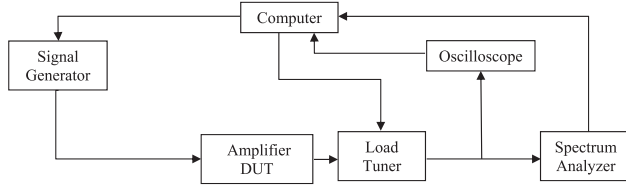


Fig. 13. Experimental setup. For these experiments, the load tuner was set to provide a 50- Ω impedance to the device under test (DUT). The computer uploads the waveform into the signal generator at each iteration of the optimization. The time-domain oscilloscope measurement is sent to the computer, which then uses the data to calculate the baseband AF. Calculation of the spectrum for comparison to the spectral mask can be performed using the spectrum analyzer or using a fast Fourier transform of the time-domain data from the oscilloscope.

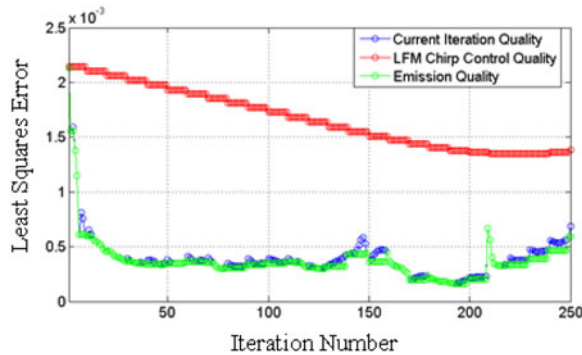


Fig. 14. Least squares distance quality for Experiment 1 (Measurement) as the algorithm iterates. The red circles show the distance quality for the control waveform, the green circles show the simulated emission, and the blue circles show the current iteration, as if T were not applied.

arbitrary waveform generator. The baseband digital waveform is then modulated to 3.3-GHz via QAM and sent to the Skyworks SKY5017-70LF InGaP-packaged amplifier. The amplifier output is then sampled by a high-frequency oscilloscope and sent back to MATLAB, where it is demodulated and analyzed. Note that this device has no relation to the simulated nonlinearities used in the simulation test of the algorithm and the results of the two will have some unrelated differences.

The same three experiments from the simulation test are used, again with a PAPR limit of 2 dB and a spectral mask constraint shown in Fig. 4. Again, each experiment continuously generates a 150-sample waveform over a period of 250 iterations, with a time support $T = 9.375 \mu\text{s}$ and frequency support $B = 8 \text{ MHz}$.

The Experiment 1 scenario shown in Fig. 7 was repeated for measurement testing. Fig. 14 shows the least squares distance quality of the waveforms as the algorithm

TABLE V
Measurement Results for Experiment 1

	Minimax		Least Squares $\cdot 10^{-3}$	
	Mean	Std. Dev.	Mean	Std. Dev.
Emission (Predistortion)	0.170	0.0677	0.372	0.200
Emission (No Predistortion)	0.181	0.0672	0.425	0.211
Control	0.689	0.0768	1.66	0.265

TABLE VI
Measurement Results for Experiment 2

	Minimax		Least Squares $\cdot 10^{-3}$	
	Mean	Std. Dev.	Mean	Std. Dev.
Emission (Predistortion)	0.188	0.0825	0.498	0.398
Emission (No Predistortion)	0.199	0.0814	0.545	0.404
Control	0.699	0.0692	1.66	0.260

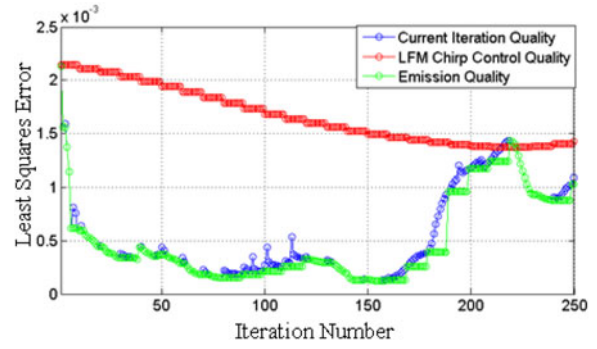


Fig. 15. Least squares distance quality for Experiment 2 (Measurement) as the algorithm iterates. The red circles show the distance quality for the control waveform, the green circles show the simulated emission, and the blue circles show the current iteration, as if T were not applied.

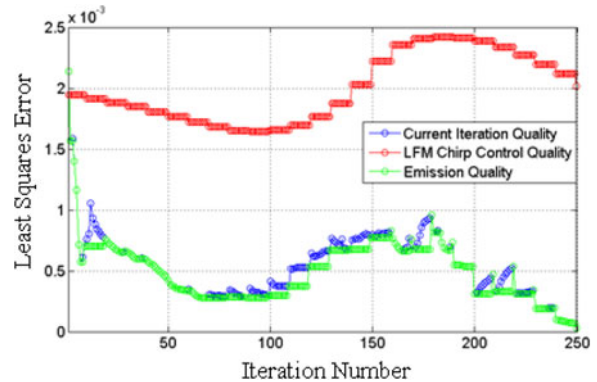


Fig. 16. Least squares distance quality for Experiment 3 (Measurement) as the algorithm iterates. The red circles show the distance quality for the control waveform, the green circles show the simulated emission, and the blue circles show the current iteration, as if T were not applied.

iterates. Table V summarizes the measured results from Experiment 1. As in the simulations, the waveform produced by the projections algorithm performs much better than the LFM chirp control waveform. Predistortion is again observed to have a noticeable effect on the AF quality.

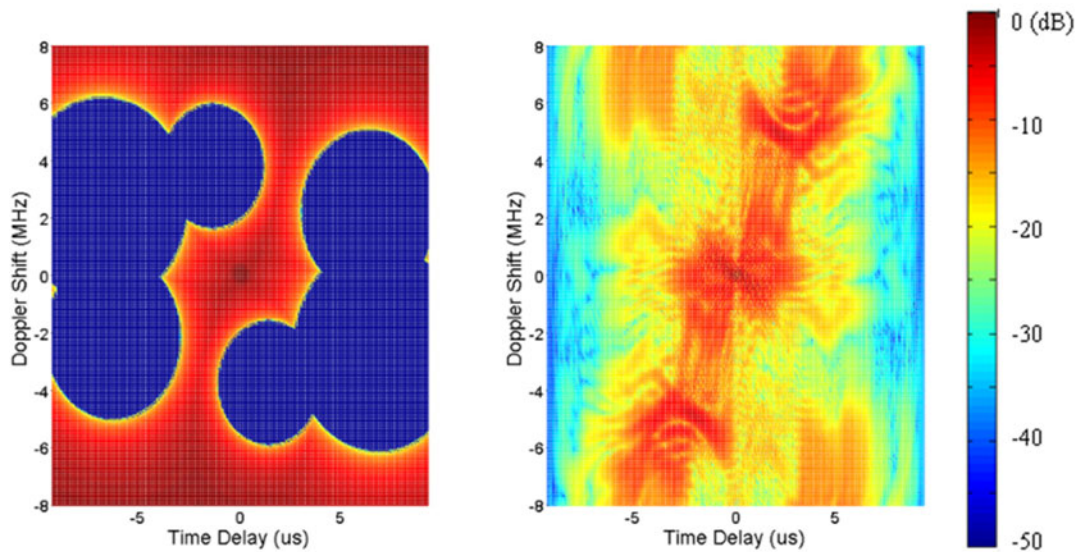


Fig. 17. Snapshot of the minimization function (left) and one of the AFs (right) associated with an emission produced by the projections algorithm in Experiment 3 (measurement).

Table VII
Measurement Results for Experiment 3

	Minimax		Least Squares $\cdot 10^{-3}$	
	Mean	Std. Dev.	Mean	Std. Dev.
Emission (Predistortion)	0.197	0.0503	0.496	0.398
Emission (No Predistortion)	0.205	0.0570	0.556	0.280
Control	0.697	0.0445	2.00	0.278

The Experiment 2 range/Doppler scenario shown in Fig. 9 was also repeated for measurement testing. Fig. 14 shows the least squares distance quality of the waveforms as the algorithm iterates, and Table VI summarizes the measured results from Experiment 2. As shown in Fig. 15, the distance function of the control waveform is lower for a small range of iterations than the waveform produced by the projections. However, this lasts for only about three iterations and the substantial difference in average values are consistent with previous results. Predistortion again results in more closely matching the AF of the transmitted waveform to the minimization function.

The range/Doppler scenario for Experiment 3, as shown in Fig. 11, was also repeated in measurement testing. Fig. 16 shows the least squares distance quality of the waveforms as the algorithm iterates, and Table VII summarizes the measured results from Experiment 3. A snapshot of an AF produced in measurement for Experiment 3 is shown in Fig. 17.

In this paper, the algorithm trials shown converge consistently. It is important to note, however, that the sets used for this alternating projections method are not necessarily convex. As such, convergence of this method, while most often achieved, is not guaranteed. However, it seems based on our experience that the algorithm converges to a useful result.

V. CONCLUSION

An alternating projections algorithm for waveform synthesis based on desired AF characteristics, spectral mask constraints, and PAPR has been presented and its results validated, using both simulation and measurement data. The algorithm synthesizes a waveform which has an optimized AF based on a given minimization function, while ensuring that the associated waveform is constrained by a given PAPR and spectral mask. In both simulation and measurement, the algorithm was shown to consistently have a better error function when compared to the minimization function than that of a commonly used radar function, the LFM chirp. In initial iterations of the experiments, the qualities of the chirp and of the projections waveform were similar; however, the projections algorithm very quickly finds waveforms which are better suited for the given minimization function. These results will allow for a radar system to dynamically adjust its waveform for dynamically changing range and Doppler of potential interferers in real time, while guaranteeing spectral compliance. The result of the optimization is a radar waveform providing good device efficiency, meeting spectral constraints, and providing desirable range/Doppler resolution. As a part of the optimization, the undesirable effects of power amplifier nonlinearities on the AF are minimized.

REFERENCES

- [1] P. M. Woodward
Probability, Information Theory and Radar. New York, NY, USA: Pergamon, 1953.
- [2] M. Cheney
A mathematical tutorial on synthetic aperture radar
SIAM Rev., vol. 43, no. 2, pp. 301–312, 2001.
- [3] D. Eustice, C. Baylis, and R. J. Marks II
Woodward's ambiguity function: From foundations to applications

- In *Proc. Texas Symp. Wireless Microw. Circuits Syst.*, Waco, TX, USA, Apr. 2015.
- [4] C. H. Wilcox
The synthesis problem for radar ambiguity functions
Mathematics Res. Center, Univ. Wisconsin, Madison, WI, USA, Tech. Rep. 157, 1960.
- [5] S. M. Sussman
Least-square synthesis of radar ambiguity functions
IRE Trans. Inf. Theory, vol. 8, pp. 246–254, 1962.
- [6] J. D. Wolf, G. M. Lee, and C. E. Suyo
Radar waveform synthesis by mean-square optimization techniques
IEEE Trans. Aerosp. Electron. Syst., vol. AES-5, no. 4, pp. 611–619, Jul. 1968.
- [7] I. Gladkova and D. Chebanov
On a new extension of wilcox’s method
WSEAS Trans. Math., vol. 3, no. 1, 2004.
- [8] I. Gladkova and D. Chebanov
On the synthesis problem for a waveform having a nearly ideal ambiguity surface
In *Proc. Int. Conf. Radar Syst.*, Philadelphia, PA, USA, 2004.
- [9] M. A. Sebt, A. Sheikhi, and M. M. Nayebi
Orthogonal frequency-division multiplexing radar signal design with optimised ambiguity function and low peak-to-average power ratio
IET Radar, Sonar, Navig., vol. 3, no. 2, pp. 122–132, 2008.
- [10] J. A. G. O. Byrnes
Computational Noncommutative Algebra and Applications: Proceedings of the NATO Advanced Study Institute on Computatoinal Noncommutative Algebra and Applications. New York, NY, USA: Springer, 2006, p. 351.
- [11] J. P. Costas
A study of a class of detection waveforms having nearly ideal range-Doppler ambiguity properties
Proc. IEEE, vol. 72, no. 8, pp. 996–1009, Aug. 1984.
- [12] L. K. Patton and B. D. Rigling
Autocorrelation constraints in radar waveform optimization for detection
IEEE Trans. Aerosp. Electron. Syst., vol. 48, no. 2, pp. 951–968, Apr. 2012.
- [13] L. K. Patton and B. D. Rigling
Phase retrieval for radar waveform optimization
IEEE Trans. Aerosp. Electron. Syst., vol. 48, no. 4, pp. 3287–3302, Oct. 2012.
- [14] L. K. Patton and B. K. Rigling
Autocorrelation and modulus constraints in radar waveform optimization
In *Proc. Int. Waveform Diversity Des. Conf.*, Kissimmee, FL, USA, Feb. 2009, pp. 150–154.
- [15] I. W. Selesnick and S. U. Pillai
Chirp-line transmit waveforms with multiple frequency-notches
In *Proc. IEEE Radar Conf.*, Kansas City, MO, USA, 2011.
- [16] I. W. Selesnick and S. U. Pillai
An iterative algorithm for the construction of notched chirp signals
In *Proc. IEEE Radar Conf.*, Washington, DC, USA, 2010.
- [17] M. Kassab, M. Lesturgie, and J. Fiorina
Alternate projections technique for radar waveform design
In *Proc. Int. Radar Conf., Surveillance Safer World*, Bordeaux, France, 2009.
- [18] J. Jakabosky, S. D. Blunt, M. R. Cook, J. Stiles, and S. Seguin
Transmitter-in-the-loop optimization of physical radar emissions
In *Proc. IEEE Radar Conf.*, Atlanta, GA, USA, May 2012.
- [19] J. Jakabosky, L. Ryan, and S. Blunt
Transmitter-in-the-loop optimization of distorted OFDM radar emissions
In *Proc. IEEE Radar Conf.*, Ottawa, ON, Canada, 2013.
- [20] S. Blunt, M. Cook, J. Jakabosky, J. de Graaf, and E. Perrins
Polyphase-coded FM (PCFM) radar waveforms, Part I: Implementation
IEEE Trans. Aerosp. Electron. Syst., vol. 50, no. 3, pp. 2218–2229, Jul. 2014.
- [21] S. Blunt, J. Jakabosky, M. Cook, J. Stiles, S. Seguin, and E. Mokole
Polyphase-coded FM (PCFM) radar waveforms, Part II: Optimization
IEEE Trans. Aerosp. Electron. Syst., vol. 50, no. 3, pp. 2230–2241, Jul. 2014.
- [22] J. Jakabosky, S. Blunt, and T. Higgins
Ultra-low sidelobe waveform design via spectral shaping and LINC transmit architecture
In *Proc. IEEE Radar Conf.*, Arlington, VA, USA, May 2015.
- [23] R. Nobakht and M. R. Civanlar
Optimal pulse shape design for digital communication systems by projections onto convex sets
IEEE Trans. Commun., vol. 43, no. 12, p. 2874, Dec. 1995.
- [24] W. Bin, Y. Wenfang, and W. Jinkuan
Adaptive waveform design for multiple radar tasks based on constant modulus constraint
J. Appl. Math., vol. 2013, 2013, Art. no. 295493.
- [25] R. Gerchberg and W. Saxton
A practical algorithm for the determination of phase from image and diffraction plane pictures
Optik, vol. 35, no. 22, pp. 237–248, 1972.
- [26] S. U. Pillai, K. Y. Li, R. Zheng, and B. Himed
Design of unimodular sequences using generalized receivers
In *Proc. IEEE Radar Conf.*, Washington, DC, USA, May 2010, pp. 729–734.
- [27] D. Eustice, C. Baylis, L. Cohen, C. Latham, and R. J. Marks II
Optimizing radar waveforms using generalized alternating projections
In *Proc. Texas Symp. Wireless Microw. Circuits Syst*, Waco, TX, USA, Apr. 2015.
- [28] D. Eustice, C. Baylis, L. Cohen, and R. J. Marks II
Waveform synthesis via alternating projections with ambiguity function, peak-to-average power ratio, and spectrum requirements
In *Proc. IEEE Radio Wireless Symp.*, Austin, TX, USA, Jan. 2016.
- [29] D. Eustice, C. Baylis, L. Cohen, and R. J. Marks II
Mythbusting: Exploring common misconceptions about the ambiguity function
In *Proc. URSI North Amer. Radio Sci. Meet.*, Vancouver, BC, Canada, Jul. 2015.
- [30] M. A. Sahib and R. Kamil
Loudspeaker nonlinearity compensation with inverse tangent hyperbolic function-based predistorter for active noise control
Trans. Inst. Meas. Control, vol. 36, no. 8, pp. 971–982, 2014.
- [31] R. Santucci, M. K. Banavar, A. Spanias, and C. Tepedenioglu
Estimation for amplify-and-forward transmissions with nonlinear amplifiers
In *Proc. Constantinides Int. Workshop Signal Process.*, 2013.
- [32] F. M. Ghannouchi and O. Hammi
Behavioral modeling and predistortion
IEEE Microw. Mag., vol. 10, no. 7, pp. 52–64, Dec. 2009.
- [33] K. J. Muhonen, M. Kavehrad, and R. Krishnamoorthy
Look-up table techniques for adaptive digital predistortion: A development and comparison
IEEE Trans. Veh. Technol., vol. 49, no. 5, pp. 1995–2002, Sep. 2000.
- [34] D. R. Morgan, Z. Ma, J. Kim, M. G. Zierdt, and J. Pastalan
A generalized memory polynomial model for digital predistortion of RF power amplifiers
IEEE Trans. Signal Process., vol. 54, no. 10, pp. 3852–3860, Oct. 2006.

Dylan Eustice received the Bachelor of Science degree in electrical and computer engineering and the Master of Science degree in electrical and computer engineering from Baylor University, Waco, TX, USA, in 2014 and 2015, respectively. He is currently with Numerica, Fort Collins, CO, USA.

Casey Latham received the Bachelor of Science degree in electrical and computer engineering from Baylor University, Waco, TX, USA, in 2016, where he is currently working toward the M.S.E.C.E. degree in electrical engineering. His research is focuses on developing a joint circuit and waveform optimization for radar transmission.



Charles Baylis (S'03–M'08–SM'16) received the B.S., M.S., and Ph.D. degrees in electrical engineering from the University of South Florida, Tampa, FL, USA, in 2002, 2004, and 2007, respectively.

He is currently an Associate Professor of electrical and computer engineering with Baylor University, Waco, TX, USA, where he directs the Wireless and Microwave Circuits and Systems Program. He has focused his work on the application of microwave circuit technology and measurements, combined with intelligent optimization algorithms, to create reconfigurable transmitters. He founded the annual Texas Symposium on Wireless and Microwave Circuits and Systems and serves as the Chair of the Executive Committee for this conference. His research focuses on spectrum issues in radar and communication systems, and has been sponsored by the National Science Foundation, the Army Research Laboratory, and the Naval Research Laboratory.

Lawrence Cohen (M'87–SM'12) received the B.Sc. degree in electrical engineering from The George Washington University, Washington, DC, USA, in 1975, and the M.Sc. degree in electrical engineering from Virginia Tech, Blacksburg, VA, USA, in 1994.

For the past 26 years, he has been with the Naval Research Laboratory, Washington, DC, USA. He has been involved in electromagnetic-compatibility (EMC) engineering and management, shipboard antenna integration, and radar system design for 33 years. In this capacity, he has worked in the areas of shipboard electromagnetic-interference problem identification, quantification and resolution, mode-stirred chamber research, and radar absorption material design, test, and integration. In March 2007, he acted as the Navy's Principal Investigator in the assessment of radar emissions on a WiMAX network. Additionally, he has acted as the Principal Investigator for various radar programs, including the radar transmitter upgrades. He is currently involved with identifying and solving spectrum conflicts between radar and wireless systems as well as research into spectrally cleaner power-amplifier designs, tube, and solid state.

Mr. Cohen is certified as an EMC Engineer by the National Association of Radio and Telecommunications Engineers. He served as the Technical Program Chairman for the *IEEE 2000 International Symposium on EMC* and was elected for a three-year term to the IEEE EMC Society Board of Directors in 1999 and 2009, respectively. He is also a Member of the IEEE EMC Society Technical Committee 6 for Spectrum Management.



Robert J. Marks II (S'71–M'72–SM'83–F'94) is currently a Distinguished Professor of electrical and computer engineering with Baylor University, Waco, TX, USA. He served for 17 years as the faculty advisor to the student chapter of Campus Crusade for Christ with the University of Washington. His most recent books are *Handbook of Fourier Analysis and Its Applications* (London, U.K.: Oxford Univ. Press, 2009), and *Biological Information—New Perspectives* (Singapore: World Scientific, 2013), coedited by M. J. Behe, W. A. Dembski, B. L. Gordon, and J. C. Sanford. He has an Erdős–Bacon number of five.

He is a Fellow of the Optical Society of America.